Multifunctional Colloids with Optical, Magnetic, and Superhydrophobic Properties Derived from Nucleophilic Substitution-Induced Layer-by-Layer Assembly in Organic Media

Miseon Yoon,[†] Younghoon Kim,[†] and Jinhan Cho*

Department of Chemical and Biological Engineering, Korea University, Anam-dong, Seongbuk-gu, Seoul 136-713, Korea. [†]These authors contributed equally to this work.

ABSTRACT We demonstrate the successful preparation of multifunctional silica colloids by coating with 2-bromo-2-methylpropionic acid (BMPA)-stabilized quantum dots (BMPA-QDs) and BMPA-stabilized iron oxide particles (BMPA-Fe_3O_4), along with amine-functionalized poly(amidoamine) (PAMA) dendrimers, using layer-by-layer (LbL) assembly based on a nucleophilic substitution (NS) reaction between the bromo and amine groups in organic media. The QDs and Fe_3O_4 nanoparticles used in this study were directly synthesized in a nonpolar solvent (chloroform or toluene), and the oleic acid stabilizers were exchanged with BMPA in the same solvent to minimize chemical and physical damage to the nanoparticles. The direct adsorption of nanoparticles *via* an NS reaction in organic solvent significantly increased the packing density of the nanoparticles in the lateral dimensions because electrostatic repulsion between neighboring nanoparticles was absent. The multifunctional colloids densely coated with nanoparticles showed excellent characteristics (*i.e.*, superparamagnetism, photoluminescence, and magneto-optical tuning properties) with long-term stability in nonpolar solvents. Furthermore, deposition of the nanocomposite colloids onto flat substrates, followed by coating with a low-surface-energy fluoroalkylsilane polymer, produced a densely packed rugged surface morphology in the colloidal films that displayed superhydrophobic properties with water contact angles greater than 150°.

KEYWORDS: layer-by-layer assembly · nucleophilic substitution reaction · magnetic nanoparticles · quantum dot nanoparticles · colloidal substrate

Functional nanocomposites, including magnetic particles (MPs) and/or quantum dots (QDs), have attracted considerable attention due to their potential applications in nonvolatile memory devices, biomedical imaging, magnetic cards, and optical display films.[1−15] In particular, adsorption of combinations of these functional nanoparticles onto large colloidal substrates can have specific technological merits for tuning the optical and magnetic properties of their constituents, and the materials can be used in emerging technologies, such as magneto-optical sensing or separation techniques. The successful preparation of such colloidal composites is achieved by synthesizing the nanoparticles (MPs and QDs) in nonpolar organic solvents, rather than in aqueous media, with the help of stabilizers, such as oleic acid. This ensures a uniform size and high crystallinity.[16−19] After synthesis, the stabilizers must be exchanged to permit immobilization of the nanoparticles onto colloidal substrates and be selected to minimize chemical or physical damage that might destroy the nanoparticles' unique properties. Nanoparticles should be densely packed onto colloidal substrates without agglomeration to achieve high performance. For example, the solution pH, nature of hydrophilic ligands, and nanoparticle size can significantly affect the quantum yield of QDs[20−22] and the magnetic properties of MPs[23−27] synthesized in water. These qualities also affect the nanoparticle dispersion stability and the quantity of nanoparticles adsorbed onto the substrates. The use of colloidal nanocomposites in various organic media requires that they can be well-dispersed in nonpolar solvents, such as toluene or hexane.

Although efforts have been made to prepare hybrid nanocomposites that include MPs and QDs, previous methods have mainly been applicable to aqueous solutions only. For example, magnetic quantum dot nanocomposites were prepared by the sol−gel method.[28] The use of sol−gel methods in the design of structurally and compositionally complex nanocomposites using organic solution processes, particularly in nonpolar solvents such as toluene, chloroform, or hexane, is difficult. As an example, core−shell colloids prepared by electrostatic layer-by-layer (LbL) assembly[29−35] displayed magnetic

* Address correspondence to jinhan71@korea.ac.kr.

Received for review February 10, 2011 and accepted June 20, 2011.

Published online June 20, 2011
10.1021/nn200538a

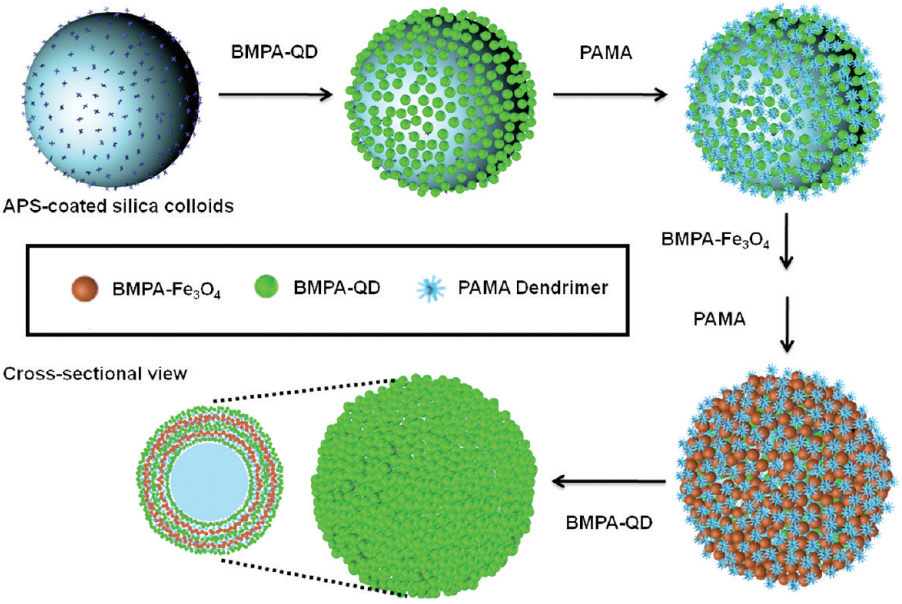

Scheme 1. Schematic for the preparation of multifunctional colloids coated with (BMPA-QD/PAMA/BMPA-Fe_3O_4)$_n$ multilayers using nucleophilic substitution reaction in organic media.

luminescent properties upon introduction of electrostatically charged Fe_3O_4 and CdTe nanoparticles.[36,37] However, the electrostatic adsorption of functional nanoparticles onto colloids usually results in a low packing density for each component layer due to electrostatic repulsion between the same charged species. To their advantage, such approaches can be used in aqueous media.

In this study, we report the preparation of multifunctional colloidal particles coated with Fe_3O_4 and CdSe@ZnS using a nucleophilic substitution (NS) reaction-based LbL assembly method in organic solvents. Hybrid nanocomposite colloids were prepared by alternate deposition of (i) superparamagnetic Fe_3O_4 (*i.e.*, BMPA-Fe_3O_4) and photoluminescent CdSe@ZnS nanoparticles (*i.e.*, BMPA-QDs), stabilized by 2-bromo-2-methylpropionic acid (BMPA) with bromo groups, in toluene; and (ii) the amine-functionalized poly(amidoamine) dendrimer (*i.e.*, PAMA) in alcohol, on silica colloidal particles *via* an NS reaction between the bromo groups of BMPA nanoparticles and the amine groups of PAMA. These colloidal composites could be well-dispersed in various organic media, such as alcohol and toluene, depending on the outermost layer deposited. We emphasize that the colloids displayed much stronger superparamagnetic and photoluminescent (PL) properties than those prepared from electrostatic LbL assembly, and these colloids displayed reversible optical tuning memory under magnetic control. Furthermore, we demonstrated that the densely packed rugged surface morphology formed from nanoparticle layers easily induced superhydrophobicity, with water contact angles exceeding 150°.

To our knowledge, this is the first report describing the preparation of the NS reaction-induced formation of multilayers on colloidal substrates in organic media (particularly nonpolar solvents). Considering that metallic nanoparticles (*i.e.*, Au, Pt, or Pd nanoparticles), which may be used as catalysts for organic synthesis or other chemical reactions in nonpolar solvent, can also be encapsulated by bromo-functionalized stabilizers,[38−41] we believe that our approach based on NS reaction-induced LbL assembly provides a method for preparing a variety of colloidal nanocomposites that function in organic solvents, and furthermore, these colloids can be used for potential applications such as magneto-optical sensing, magnetically controllable QD display, or magnetically retrievable catalytic colloids.

RESULTS AND DISCUSSION

Optical Properties. Oleic-acid-stabilized CdSe@ZnS QD nanoparticles displaying blue (PL λ_{max} = 445 nm), green (PL λ_{max} = 523 nm), and red (PL λ_{max} = 638 nm) emission bands were prepared in toluene (see the Methods section and Supporting Information, Figure S1). The initial oleic acid stabilizers were replaced with BMPA *via* ligand exchange to produce BMPA-QDs. The relative quantum yields of the blue, green, and red BMPA-QDs were measured to be 45% (relative to 9,10-diphenylanthracene), 45% (relative to coumarin 545), and 42% (relative to Rhodamine 101), respectively.

The bromo groups of BMPA stabilizers can undergo NS reaction with amino groups to covalently bond the BMPA-QDs to the amine-functionalized material, such as PAMA or aminopropyltrimethoxysilane (*i.e.*, APS). Covalent bonding was confirmed by Fourier transform infrared (FTIR) spectroscopy of the PAMA/BMPA-QD multilayer films prepared on the Si wafer substrates (see Supporting Information, Figure S2). The C−H symmetric deformation (1380 cm^{-1}) of CH_3 groups as

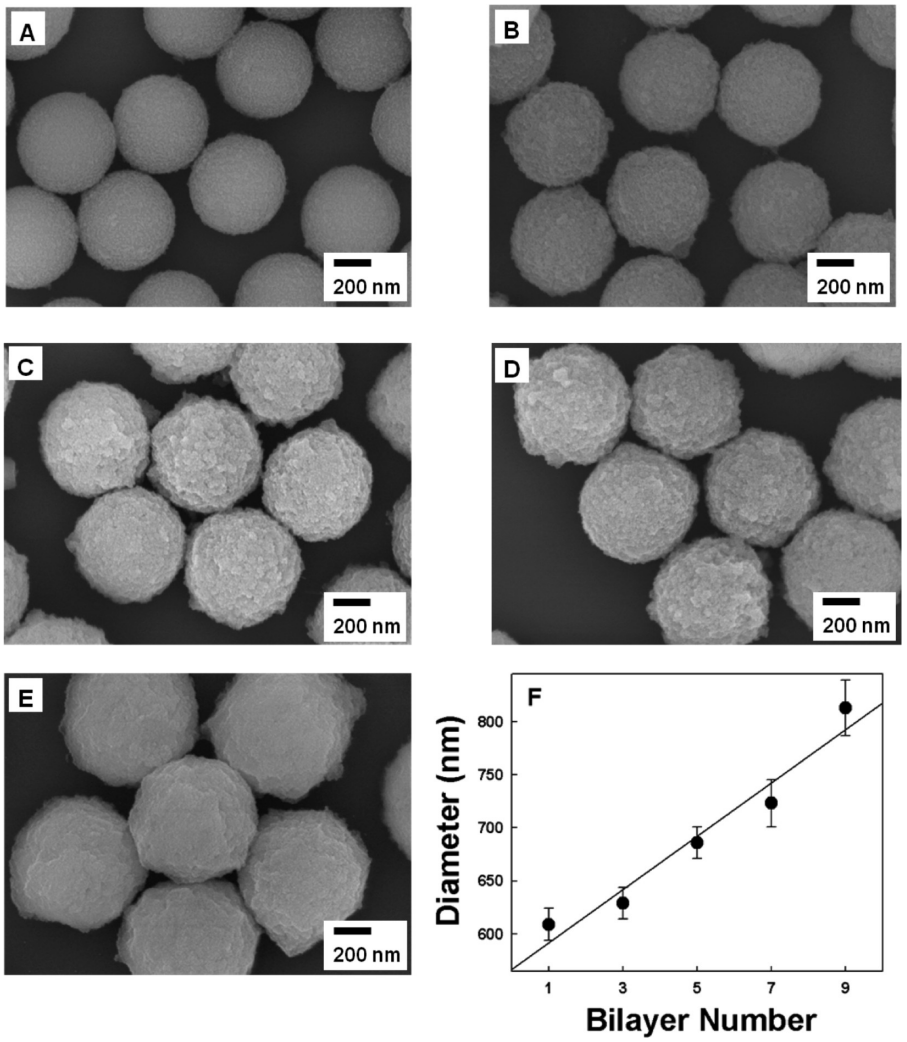

Figure 1. SEM images of APS-SiO_2 colloids coated with (BMPA-QD_{green}/PAMA)$_n$ multilayers for (A) n = 1, (B) 3, (C) 5, (D) 7, and (E) 9. (F) Size change of (BMPA-QD_{green}/PAMA)$_n$ multilayer-coated silica colloids measured with increasing bilayer number (n).

well as C═O vibration modes (1710 and 1410 cm^{-1}) were observed in BMPA-QDs. This observation implies the presence of BMPA stabilizers onto the QD because BMPA has $-CH_3$ and $-COOH$. The PAMA dendrimer has absorbance peaks caused by the characteristic C═O stretching (1629 cm^{-1}) of amide groups and N−H bend (1550 cm^{-1}) of primary amines, $-NH_2$ (see Supporting Information, Figure S2). On the other hand, the FTIR spectrum of PAMA/BMPA-QD multilayers displayed the peak broadening in the range of 1589−1500 cm^{-1}, and furthermore, the strong peaks at 1450, 1190, and 1100 cm^{-1} are caused by secondary aliphatic amines occurring from a nucleophilic substitution reaction between primary amine and bromo groups.[11]

On the basis of these results, BMPA-QDs_{green} were first deposited onto an APS-coated silica colloid (APS-SiO_2) surface, using 600 nm diameter colloidal particles, and PAMA was subsequently adsorbed onto the BMPA-QD_{green}-coated colloids. Scheme 1 schematically depicts the colloidal nanocomposite coated with (BMPA nanoparticle/PAMA)$_n$ multilayers bonded *via* nucleophilic substitution in organic media. As shown in Figure 1, a densely coated nanoparticle layer was obtained from adsorption of a single BMPA-QD_{green} layer. Increasing the bilayer number (n) from 1 to 9 produced a (BMPA-QD_{green}/PAMA)$_n$ multilayer-coated colloid layer with a more rugged and densely coated structure and without aggregation of the colloids. Although the number density of BMPA-QDs_{green} on the colloidal substrate could not be determined precisely, the frequency change of a quartz crystal microbalance (QCM) contacted with a flat substrate permitted approximation of the quantity of BMPA-QD_{green} adsorbed onto 600 nm sized colloids with the surface area of about 1.13×10^{-8} cm^2. The average frequency change of the QCM, in going from the PAMA layer to the BMPA-QD_{green} layer, was 221 Hz (3904 ng·cm^{-2}) (see Methods). The densities of the 4 nm diameter CdSe QD core and the 1 nm diameter ZnS QD shell were 5.81 and 3.89 g/cm^3, respectively. Therefore, the mass of one nanoparticle was measured to be about 5.04×10^{-10} ng, and furthermore, the number of

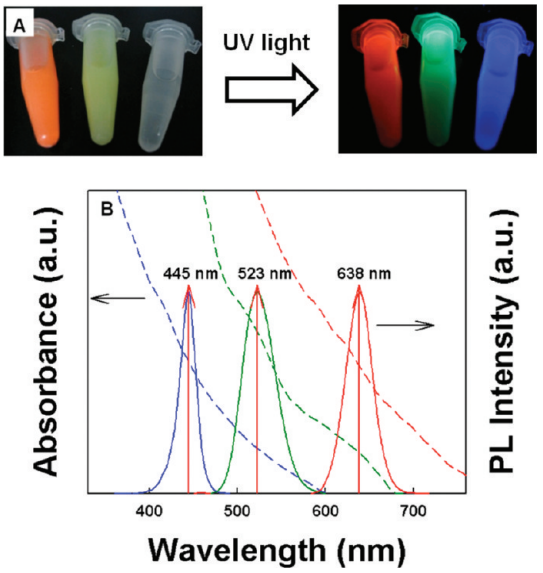

Figure 2. PL images of (BMPA-QD/PAMA)$_n$ multilayer-coated colloids. (A) Photographic images, (B) UV−vis and PL spectra of (size-controlled BMPA-QD/PAMA)$_9$ multilayer-coated SiO_2 colloids in toluene.

adsorbed QDs per unit area (cm^{-2}) measured from QCM was about 7.74×10^{12} cm^{-2}. As a result, the number of BMPA-QDs$_{green}$ adsorbed onto the colloids with the surface area of about 1.13×10^{-8} cm^2 was calculated to be about 87 500 per silica colloid. Additionally, the diameter of the functionalized colloids increased from 609 to 813 nm as the bilayer number (n) increased from 1 to 9 (Figure 1F). The nanocomposite colloids in chloroform displayed strong PL behavior with a negligible red shift in the optical spectra relative to the spectra of the oleic-acid-stabilized QDs in the same solvent (Figure 2).

For comparison, we prepared negatively charged CdSe@ZnS QDs stabilized by mercaptoacetic acid (MAA), abbreviated MAA-QD, *via* ligand exchange. Multilayered films were then prepared by LbL growth of the MAA-QD$_{green}$/cationic poly(allylamine hydrochloride) (PAH) on the anionic SiO_2 colloids *via* electrostatic deposition (see Methods). The relative quantum yield of MAA-QD$_{green}$ was measured to be 9%. Although the solution concentration and deposition layer number (9 layers) of the MAA-QD films were identical to those of the BMPA-QD films, the surface coverage of MAA-QDs on the colloids was extremely low due to long-range electrostatic repulsion between similarly charged MAA-QDs$_{green}$ (see the Supporting Information, Figure S3). These observations were in stark contrast to the trends observed for the (BMPA-QD$_{green}$/PAMA)$_n$-coated SiO_2. The PL intensity of (BMPA-QD$_{green}$/PAMA)$_9$-coated colloids, therefore, was much higher than that of the (PAH/MAA-QD$_{green}$)$_9$-coated colloids mainly due to the relatively high quantum yield of BMPA-QD$_{green}$ and their dense surface coverage per layer (Figure 3A). Remarkably, the PL intensity of (BMPA-QD$_{green}$/PAMA)$_n$

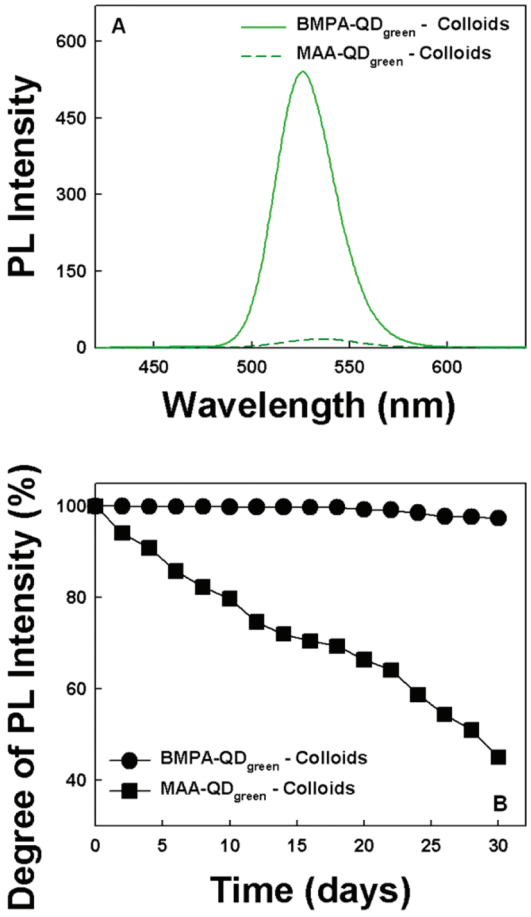

Figure 3. Intensity and stability of PL. (A) PL data and (B) change in degree of PL intensity ($\lambda_{max} \sim 523$ nm) of (BMPA-QD$_{green}$/PAMA)$_9$ and (PAH/MAA-QD$_{green}$)$_9$ multilayer-coated colloids.

multilayer-coated SiO_2 colloids was nearly unchanged during storage under ambient conditions (in the dark in ambient air) for more than 1 month, whereas the PL intensity of (PAH/MAA-QD$_{green}$)$_n$-coated colloids decreased notably depending on the storage time (Figure 3B). These results suggest that the hydrophobic character of the BMPA-QD layers deposited in nonpolar solvents prevented PL quenching by hydrolysis and oxidation under ambient conditions and preserved the original PL behavior of the QDs in the multilayer films. Recently, Tetsuka *et al.* reported that nanocomposite films composed of QDs and clay exhibited high luminescence due both to the removal of water from the film and to the excellent protective environment of the clay host.[42] Furthermore, the dispersion stability of (BMPA-QD$_{green}$/PAMA)$_n$ multilayer-coated silica colloids in various solvent strongly depends on the deposited top layer (see Supporting Information, Figure S4). If the PAMA is deposited as a top layer, these colloids can be well-dispersed in polar organic solvent such as ethanol or methanol as well as nonpolar solvent. On the other hand, if BMPA-QDs are used as a top layer, the formed colloids can be well-dispersed in toluene,

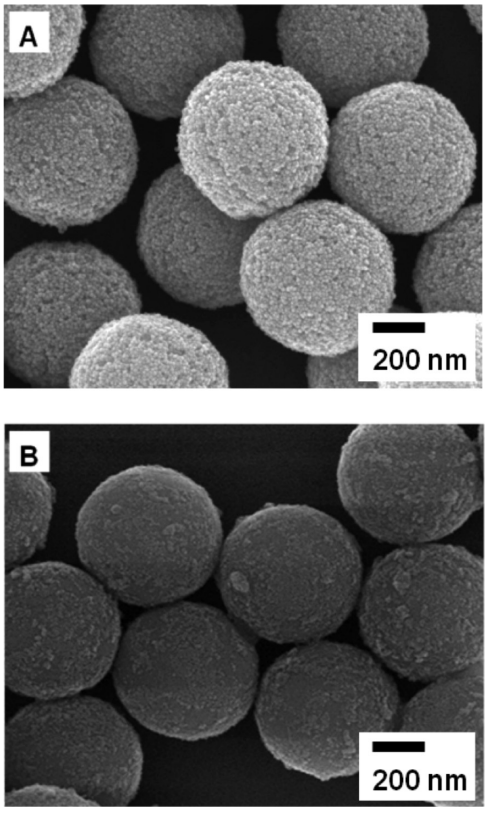

Figure 4. SEM images of (BMPA-Fe_3O_4/PAMA)$_5$ and (PAH/octakis-Fe_3O_4)$_5$ multilayer-coated silica colloids.

chloroform, 3-dimethylformamide (DMF), or 4-tetrahydrofuran (THF) for long storage time. We also observed that these colloids are highly stable without any colloidal aggregations at relatively high temperature of about 60 °C (below boiling temperature of organic media) although PL intensity of the QD is slightly decreased at elevated temperature due to their PL quenching (see Supporting Information, Figure S5).

Furthermore, in order to quantitatively investigate the stability of multilayers in aqueous solution at different solution pH, time, and temperature, the frequency change of multilayer-coated gold electrodes was measured using QCM (see Supporting Information, Figure S6). In this case, the partial deconstruction of PAMA/BMPA-QD multilayers was accelerated by decreasing the solution pH from 12 to acidic condition at 90 °C because an excess of neutral NH_2 groups of PAMA unbound to BMPA-QDs was converted to positively charged $-NH_3^+$ groups inducing the electrostatic repulsion between same charged groups with decreasing solution pH. However, in the case of other polar organic solvents (*i.e.*, isopropyl alcohol) of about 75 °C, it was observed that the stability of multilayers was maintained without any frequency change.

Magnetic Properties. The BMPA-Fe_3O_4 nanoparticles prepared by ligand exchange of BMPA on oleic-acid-stabilized 12 nm diameter Fe_3O_4 nanoparticles (see the Methods section) were also deposited on the APS-coated silica colloids to introduce magnetic properties (Figure 4A). The number of adsorbed BMPA-Fe_3O_4 particles per bilayer was measured to be approximately 9800 on the colloid, based on the following information: the adsorbed mass (Δm) of BMPA-Fe_3O_4 on the flat substrate calculated from QCM measurements, 4064 ng·cm^{-2}, the density of Fe_3O_4, 5.1 g·cm^{-3}, and the nanoparticle number density, 8.69×10^{11} cm^{-2}. The quantity of nanoparticles adsorbed onto a curved surface was assumed to be comparable to that adsorbed onto a flat surface. It should be noted that the number of adsorbed BMPA-Fe_3O_4 nanoparticles on the colloid layer was significantly higher (3328 per bilayer) than that of water-dispersible pentacyclooctasiloxane octakis (PSS) hydrate-octakis(tetramethylammonium)-stabilized Fe_3O_4 (*i.e.*, octakis-Fe_3O_4) prepared by stabilizer exchange from oleic acid to the negatively charged octakis (Figure 4B and the Methods section). As mentioned, the electrostatically charged nanoparticles imposed limitations on the nanoparticle packing density in the lateral dimensions due to electrostatic repulsion between neighboring nanoparticles at a given solution pH (*i.e.*, pH > 7 for the stable octakis-Fe_3O_4 dispersion). Although the packing density of the octakis-Fe_3O_4 could be increased by decreasing the charge density on the nanoparticles (at a solution pH < 7), the low charge density caused aggregation of the nanoparticles in solution. Aggregation made it difficult to control the preparation of stable nanocomposite colloidal coatings.

Magnetic characterization of the samples APS-SiO_2/(BMPA-Fe_3O_4/PAMA)$_9$ was performed using a superconducting quantum interference device (SQUID) magnetometer in the field range from −6000 to +6000 Oe. The magnetization curves of the multilayered films measured at room temperature (T = 300 K) were reversible without coercivity, remanence, or hysteresis, suggesting typical superparamagnetic behavior (Figure 5A). These results were confirmed by recording the magnetization at 1 min intervals at low applied fields, as shown in the inset of Figure 5A. On the other hand, at liquid helium temperature (T = 5 K), the thermally activated magnetization flipping properties of the BMPA-Fe_3O_4 revealed frustrated superparamagnetic properties. That is, the magnetization curves acquired a loop shape with distinct separation between the two sweeping directions typically observed for ferromagnets. The coercivities (H_c) and remanences (M_r) were measured to be 225 Oe and 0.0673 emu, respectively (Figure 5B). Figure 5C shows the temperature dependence of the magnetization of the resulting BMPA-Fe_3O_4-coated colloids, from 300 to 5 K, under an applied magnetic field of 150 Oe. The blocking temperature, which began to deviate between zero-field-cooling (ZFC) and field-cooling (FC) magnetization states, was fixed at approximately 150 K. These results indicate that the nanocomposite colloids coated with

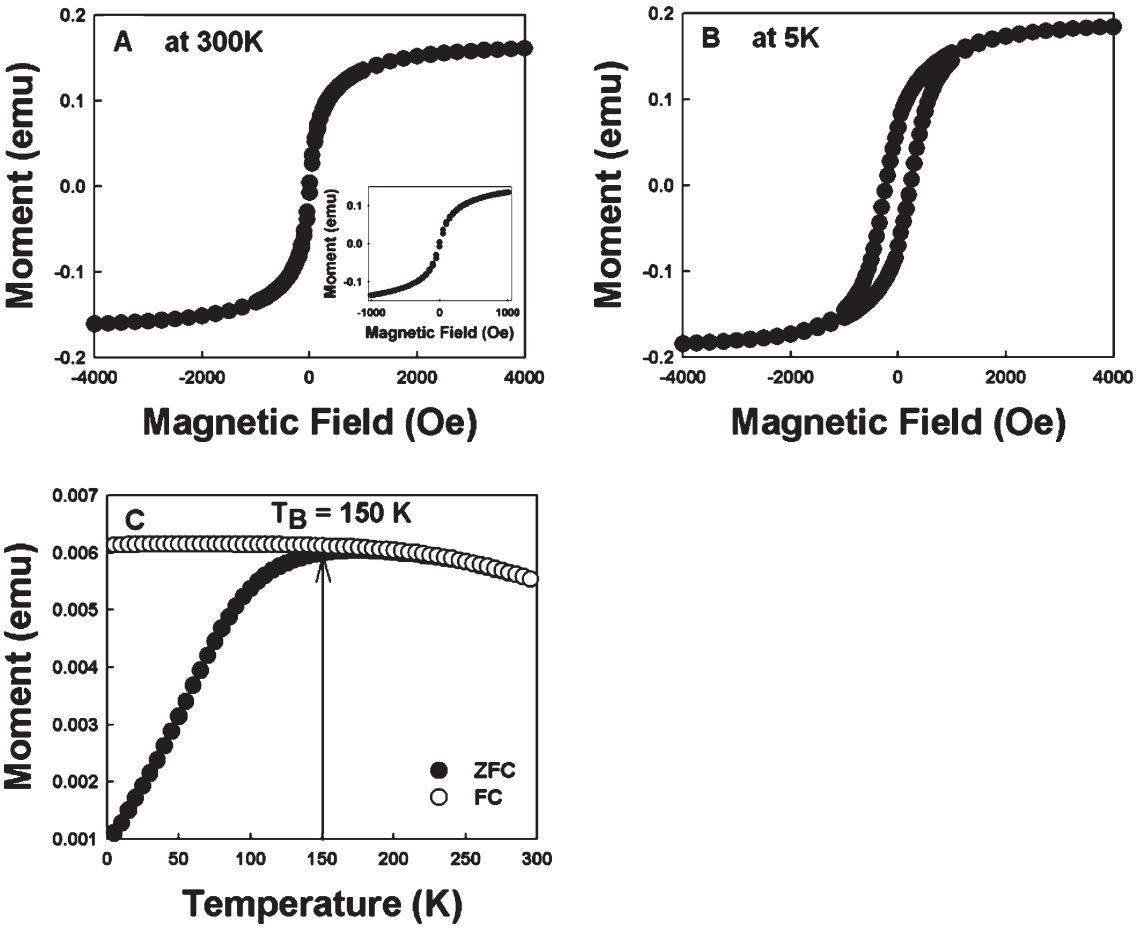

Figure 5. Magnetic curves of (PAMA/BMPA-Fe_3O_4)$_9$ multilayer-coated colloids measured at (A) 300 K and (B) 5 K. (C) Temperature dependence of zero-field-cooling (ZFC) and field-cooling (FC) magnetization measured at 150 Oe.

BMPA-Fe_3O_4 maintained their inherent superparamagnetic properties. In contrast, the magnetic colloids prepared by electrostatic LbL-assembled cationic (poly(allylamine hydrochloride) (PAH)/anionic octakis-Fe_3O_4)$_9$ had notably low degrees of saturated magnetization compared to the (PAMA/BMPA-Fe_3O_4)$_9$-coated colloids (see the Supporting Information, Figure S7). This low magnetization resulted mainly from the small quantity of octakis-Fe_3O_4 nanoparticles adsorbed onto the colloids.

Magneto-Optical Properties. Because both the highly photoluminescent QDs and the strongly superparamagnetic nanoparticles could be successfully adsorbed onto colloids *via* NS reaction without producing colloidal aggregation, the combination of these two nanoparticles may produce magneto-optically separable colloids that are stable in various organic media, including polar (alcohol) and nonpolar (toluene or chloroform) solvents. These "smart" colloids were prepared by sequential deposition of BMPA-QD_{red} and BMPA-Fe_3O_4 nanoparticles onto APS-coated silica colloids to produce APS-SiO_2/(BMPA-Fe_3O_4/PAMA/BMPA-QD_{red}/PAMA)$_3$. The resultant magnetic luminescent colloids were mixed with BMPA-QD_{green}-coated colloids without BMPA-Fe_3O_4 nanoparticles (APS-SiO_2/(BMPA-QD_{green}/PAMA)$_3$)) in a nonpolar solvent (the mass ratio of the magnetic luminescent colloids to the BMPA-QD_{green}-coated colloids was 1:1). As shown in Figure 6, the PL spectrum of the initial colloid solution showed two different PL peaks, λ_{max} = 523 or 638 nm, originating from the BMPA-QD_{green} and BMPA-QD_{red}, respectively, without indication of Förster energy transfer. When a hand-held magnet was placed close to the glass vial, the magnetic photoluminescent colloids that emitted in the red were quickly attracted to the magnet and accumulated near it within a few minutes. The remaining solution displayed green emission due to the dispersed BMPA-QD_{green}-coated colloids without BMPA-Fe_3O_4, under UV light irradiation. The PL spectrum of the solution remaining after application of an external magnetic field did not display the red emission band in its spectrum. These results showed that the blending solution of photoluminescent colloids with and without BMPA-Fe_3O_4 can display reversible optically tuned properties under magnetic control in nonpolar solvent.

Superhydrophobicity. Silica colloids densely coated with nanoparticles were deposited onto flat substrates, followed by introduction of fluoroalkylsilane, to prepare superhydrophobic surfaces with hierarchical dual roughness (micrometer-scale as well as nanometer-

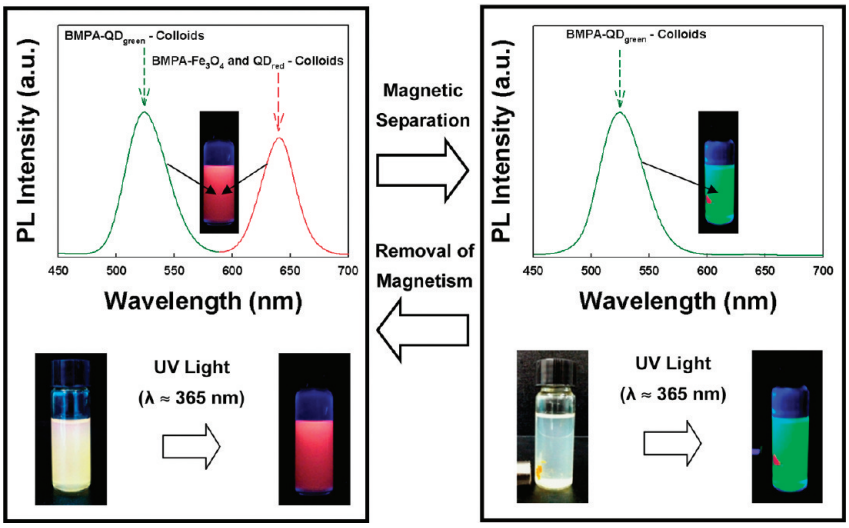

Figure 6. Photographic and SEM images of magnetically separable colloids displaying photoluminescent properties. In this case, the solution was blended with two different kinds of colloids coated with (BMPA-Fe_3O_4/PAMA/BMPA-QD_{red}/PAMA)$_3$ and (BMPA-QD_{green}/PAMA)$_3$ multilayers, respectively.

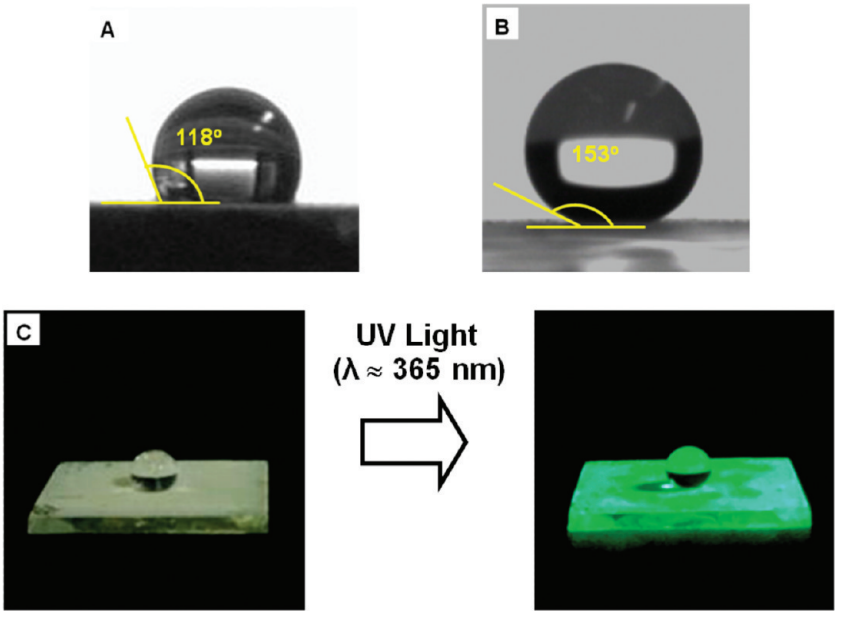

Figure 7. Superhydrophobicity of PAMA/BMPA nanoparticle multilayer-coated colloidal films. Water droplet on (A) silica colloidal films without nanoparticles and (B) (BMPA-Fe_3O_4/PAMA/BMPA-QD_{green}/PAMA)$_3$ multilayer-coated silica colloidal films. In this case, the water contact angles obtained from bare and multilayer-coated colloidal films were measured to be about (A) 118° and (B) 153°, respectively. (C) Photographic image of superhydrophobic surface prepared from magnetic luminescent colloidal films. Note that for samples in (A–C), the outermost surface of colloidal films was coated with fluoroalkylsilane polymer.

scale roughness).[43–49] These superhydrophobic films also displayed optical and magnetic properties *via* the hydrophobic quantum dots and magnetic nanoparticles. Several reports have described the preparation of multifunctional superhydrophobic films that permit modulation of the water contact angle or UV light-driven optical properties. However, smart superhydrophobic films with nanometer-scale roughness, formed by the adsorption of inherently multifunctional nanoparticles, have not been described to date. Figure 7A shows the water contact angles of silica colloidal films with and without adsorbed BMPA-stabilized nanoparticles. The fluoroalkylsilane-coated colloidal films without nanoparticles yielded a water contact angle of 118°. On the other hand, colloidal films with BMPA-QD and Fe_3O_4 displayed a water contact angle exceeding 150°, in addition to its strong PL and magnetic properties. The hierarchical surface of a colloidal film prepared from BMPA-stabilized nanoparticles lies in the Cassie state[44] in that $\Delta\theta_{ad\text{-}re}$ is smaller than 10°. These results indicate

that BMPA-stabilized nanoparticles could be used to form structural features that displayed superhydrophobicity in addition to the integrated functionalities of PL and superparamagnetism. It should be noted that the functional colloids were easily prepared by an NS reaction-based LbL assembly that facilitated adsorption of densely packed nanoparticles with retention of the inherent properties. We emphasize that the present approach of incorporating 600 nm silica colloids and BMPA-stabilized nanoparticles is not limited to the system mentioned here. It may be extended to other general areas by incorporating a variety of functional particles, such as metal nanoparticles or nanowires.

CONCLUSIONS

We demonstrated that multifunctional colloids coated with (PAMA/BMPA-Fe_3O_4)$_n$ or/and (PAMA/BMPA-CdSe@ZnS)$_n$ multilayers could be successfully prepared using a NS reaction-based LbL assembly method in organic media. Coating of BMPA-Fe_3O_4 or PAMA as an outermost layer produced well-dispersed colloids in nonpolar solvents (toluene or chloroform) or in polar organic solvents (alcohol). These colloids revealed strong magnetic and photoluminescent properties due to the presence of densely coated nanoparticles (BMPA-Fe_3O_4 and BMPA-CdSe@ZnS). The colloids additionally revealed high efficiency as a result of the crystal quality, functional stability, and dense coating of BMPA nanoparticles. We showed that the magnetic photoluminescent colloids provided reversible optical tuning memory under an external magnetic field. The highly protuberant and rugged surface morphology produced by the nanoparticle-coated colloids generated superhydrophobicity with a water contact angle exceeding 150°.

METHODS

Materials. Poly(amidoamine) (*i.e.*, PAMA) dendrimer (core type: ethylene diamine), pentacyclooctasiloxane octakis (PSS) hydrate-octakis(tetramethylammonium) (*i.e.*, octakis), oleic acid, 2-bromo-2-methylpropionic acid (BMPA), CdO, zinc acetate, 1-octadecene, selenium, sulfur powder, and trioctylphosphine poly(allylamine hydrochloride) (*i.e.*, PAH) were purchased from Sigma Aldrich. Oleic-acid-stabilized CdSe@ZnS with blue, green, and red-pink emissive colors were synthesized as previously reported by Bae *et al.*[50] For blue emissive QDs, 38.5 mg of CdO, 700 mg of zinc acetate, 17.6 mL of oleic acid, and 15 mL of 1-octadecene were put into a 250 mL round flask. The mixture was heated to 150 °C with N_2 gas blowing and further heated to 300 °C to form a clear solution of $Cd(OA)_2$ and $Zn(OA)_2$. At this temperature, 31 mg of Se powder and 128.2 mg of S powder both dissolved in 2 mL of trioctylphosphine were quickly injected into the reaction flask. After the injection, the temperature of the reaction flask was set to 300 °C for promoting the growth of QDs, and it was then cooled to room temperature to stop the growth. QDs were purified by adding 20 mL of chloroform and an excess amount of acetone (3 times). After this purification, 3.34 wt % of BMPA was added to 40 mL QD solution for the stabilizer exchange from oleic acid to BMPA and then was heated at 40 °C for 2 h.

In the case of mercaptoacetic acid (MAA)-QDs, 15 mg·mL^{-1} of oleic-acid-stabilized QDs in 5 mL of toluene was mixed with 10 mL of aqueous solution containing 100 mg·mL^{-1} of MAA at 45 °C. The MAA-QD obtained from phase transfer was precipitated by the addition of excess ethanol solvent and centrifugation at 6000 rpm for 6 min. The precipitated MAA-QDs were redispersed in aqueous solution at pH 9. The concentration of MAA-QD was adjusted to 1 mg·mL^{-1}.

Oleic-acid-stabilized Fe_3O_4 of about 12 nm size was synthesized in toluene as previously reported by the Hyeon group.[16] BMPA (1.336 g, 8 mmol) was added to 40 mL of Fe_3O_4 solution for the stabilizer exchange from oleic acid to BMPA and then was heated at 40 °C for 2 h. Octakis-Fe_3O_4 was prepared by the stabilizer exchange from oleic acid to octakis. In this case, a total of 100 mg of oleic acid-Fe_3O_4 was dissolved in 7.5 mL of toluene, and 750 mg of excess octakis was dissolved in 7.5 mL of pH 9 water.

Buildup of Multilayers on Colloidal Substrate. The concentration of PAMA, BMPA-QD, and BMPA-Fe_3O_4 solutions used for all the experiments was fixed to 1 mg·mL^{-1} in organic media (ethanol for PAMA and toluene for BMPA-Fe_3O_4). The (PAMA/BMPA-QD or BMPA-Fe_3O_4)$_n$ multilayer-coated silica colloids were prepared as follows: 100 μL of a concentrated dispersion (6.4 wt %) of negatively charged 600 nm silica colloids was diluted to 0.5 mL with deionized water. After fast centrifugation (8000 rpm, 5 min) of colloidal solution, supernatant water was removed, and then 1 mg·mL^{-1} of aminopropyltrimethoxysilane (APS) ethanol solution was added to silica colloidal sediment followed by ultrasonication and sufficient adsorption time. Excess APS was removed by three centrifugations (8000 rpm, 5 min)/wash cycles. For the preparation of multilayers onto APS silica colloids, 0.5 mL of BMPA-QD (or Fe_3O_4) (1 mg·mL^{-1}) in toluene was added, and after deposition during 10 min, the excess BMPA-QD was removed by three centrifugations as mentioned above. Then, 0.5 mL of PAMA (1 mg·mL^{-1}) in ethanol was then deposited onto the BMPA-QD-coated colloids using the same conditions. The above process was repeated until the desired layer number was deposited on the colloidal silica.

Buildup of Multilayers on Planar Substrate. The toluene or hexane dispersion of BMPA-QDs (or BMPA-Fe_3O_4) and the ethanol solution of PAMA were prepared at the concentration of 1 mg·mL^{-1}. Prior to LbL assembly, quartz, silicon, or quartz crystal microbalance (QCM) gold substrates were cleaned by RCA solution ($H_2O/NH_3/H_2O_2$ 5:1:1 v/v/v). These substrates were first dipped in the PAMA solution for 10 min, followed by washing twice with ethanol and drying with a gentle stream of nitrogen. The PAMA-coated substrates were dipped into the dispersions of BMPA-QDs (or BMPA-Fe_3O_4) for 20 min, followed by washing with toluene and drying with nitrogen. The resulting substrates were dipped in the PAMA solution for 10 min. The above dipping cycles were repeated until the desired layer numbers were obtained.

Measurements. Fourier transform infrared (FTIR) spectra were taken with a FTIR-200 spectrometer (JASCO Corporation). For this measurement, BMPA-Fe_3O_4, PAMA dendrimer, and (PAMA/BMPA-Fe_3O_4)$_n$ multilayers were deposited onto NaCl substrates.

UV−vis and PL spectra were measured with a Perkin-Elmer Lambda 35 UV−vis spectrometer and a fluorescence spectroscope (Perkin-Elmer LS 55), respectively. The PL spectra of (PAMA/BMPA-QD)$_n$ multilayers were measured at an excitation wavelength of $\lambda_{ex} \approx 300$ nm.

A QCM device (QCM200, SRS) was used to investigate the mass of material deposited into flat gold electrodes. The resonance frequency of the QCM electrodes was *ca.* 5 MHz. The adsorbed mass of PAMA, BMPA-QDs, and BMPA-Fe_3O_4, octakis-Fe_3O_4, Δm, can be calculated from the change in QCM frequency, ΔF, according to the Sauerbrey equation:[51] ΔF (Hz) = $-56.6 \times \Delta m_A$, where Δm_A is the mass change per quartz crystal unit area, in μg·cm^{-2}. Although it was reported by Kasemo and co-workers that the Sauerbrey equation between adsorbed mass and frequency change has much difficulty being applied to the viscoelastic, thicker or hydrogel layers containing water

molecules at the solid−liquid interface,[52−55] the QCM measurements in our study were made after sufficiently drying the adsorbed layer using nitrogen gas. Additionally, the frequency changes contributed by PAMA were measured to be below 5% compared to those of inorganic nanoparticles (*i.e.*, BMPA-QD and BMPA-Fe_3O_4), and furthermore, the thickness of PAMA is below 2 nm per layer. Therefore, PAMA/BMPA nanoparticle multilayers adsorbed on the crystal surface can be regarded as rigid, evenly distributed, and sufficiently thin films satisfying the Sauerbrey equation.

The magnetism of $(PAMA/BMPA\text{-}Fe_3O_4)_n$ multilayers was measured by a superconducting quantum interference device (SQUID, MPMS5) magnetometer.

Preparation of Superhydrophobic Films. Quartz substrate was dipped into 0.1 wt % PAMA/BMPA-QD/PAMA/Fe_3O_4 multilayer-coated silica colloidal toluene solution for 30 s and then dried without any gas stream. The hydrophobization of the convectively assembled multilayer-coated silica colloidal films onto quartz substrates was performed by dipping the films in *n*-hexane solution containing the 1*H*,1*H*,2*H*,2*H*-perfluorotrichlorosilane (Aldrich) (6 mg·mL^{-1}) for 20 min and then followed by mild baking at 70 °C for 30 min under vacuum.

Acknowledgment. This work was supported by the National Research Foundation (NRF) grants funded by the Korea government (MEST) (2010-0029106, 2010-0027751) and ERC Program of NRF grant funded by the Korea government (MEST) (R11-2005-048-00000-0).

Supporting Information Available: TEM images and FTIR spectra of oleic acid-QDs; SEM images of $(PAMA/MAA\text{-}QD)_9$ multilayer-coated colloids; dispersion stability of multilayer-coated colloids; degree of frequency change of multilayers; magnetism curves of $(PAH/octakis\text{-}Fe_3O_4)_9$ multilayer-coated colloids. This material is available free of charge *via* the Internet at http://pubs.acs.org.

REFERENCES AND NOTES

1. Huang, X.; Bronstein, L. M.; Retrum, J.; Dufort, C.; Tsvetkova, I.; Aniagyei, S.; Stucky, G.; McKenna, B.; Remmes, N.; Baxter, D.; *et al.* Self-Assembled Virus-like Particles with Magnetic Cores. *Nano Lett.* **2007**, *7*, 2407–2416.
2. Kim, J.; Lee, J. E.; Lee, J.; Jang, Y.; Kim, S.-W.; An, K.; Yu, J. H.; Hyeon, T. Generalized Fabrication of Multifunctional Nanoparticle Assemblies on Silica Spheres. *Angew. Chem.* **2006**, *118*, 4907–4911.
3. Speliotis, D. E. Magnetic Recording beyond the First 100 Years. *J. Magn. Magn. Mater.* **1999**, *193*, 29–35.
4. Bae, S.-S.; Lim, D. K.; Park, J.-I.; Lee, W.-R.; Cheon, J.; Kim, S. Selective Assembled Co Nanoparticle Stripes Prepared by Covalent Linkage and Microcontact Printing. *J. Phys. Chem. B* **2004**, *108*, 2575–2579.
5. Kim, Y.; Lee, C.; Shim, I.; Cho, J. Nucleophilic Substitution Reaction Based Layer-by-Layer Growth of Superparamagnetic Nanocomposite Films with High Nonvolatile Memory Performance. *Adv. Mater.* **2010**, *22*, 5140–5144.
6. Coe, S.; Woo, W. K.; Bawendi, M.; Bulovic, V. Electroluminescence from Single Monolayers of Nanocrystals in Molecular Organic Devices. *Nature* **2002**, *420*, 800–803.
7. Zhang, H.; Cui, Z.; Wang, Y.; Zhang, K.; Ji, X.; Lu, C.; Yang, B.; Gao, M. From Water-Soluble CdTe Nanocrystals to Fluorescent Nanocrystal−Polymer Transparent Composites Using Polymerizable Surfactants. *Adv. Mater.* **2003**, *15*, 777–780.
8. Wang, D.; Rogach, A. L.; Caruso, F. Composite Photonic Crystals from Semiconductor Nanocrystal/Polyelectrolyte-Coated Colloidal Spheres. *Adv. Mater.* **2003**, *15*, 2724–2729.
9. Wang, W.; Rogach, A. L.; Caruso, F. Semiconductor Quantum Dot-Labeled Microsphere Bioconjugates Prepared by Stepwise Self-Assembly. *Nano Lett.* **2002**, *2*, 857–861.
10. Braun, M.; Burda, C.; El-Sayed, M. A. Variation of the Thickness and Number of Wells in the CdS/HgS/CdS Quantum Dot Quantum Well System. *J. Phys. Chem. A* **2001**, *105*, 5548–5551.
11. Lee, B.; Kim, Y.; Lee, S.; Kim, Y. S.; Wang, D.; Cho, J. Layer-by-Layer Growth of Polymer/Quantum Dot Composite Multilayers by Nucleophilic Substitution in Organic Media. *Angew. Chem., Int. Ed.* **2010**, *49*, 359–363.
12. Erogbogbo, F.; Yong, K.-T.; Hu, R.; Law, W.-C.; Ding, H.; Chang, C.-W.; Prasad, P. N.; Swihart, M. T. Biocompatible Magnetofluorescent Probes: Luminescent Silicon Quantum Dots Coupled with Superparamagnetic Iron(III) Oxide. *ACS Nano* **2010**, *4*, 5131–5138.
13. Krusin-Elbaum, L.; Shibauchi, T.; Argyle, B.; Gignac, L.; Weller, D. Stable Ultrahigh-Density Magneto-Optical Recordings Using Introduced Linear Defects. *Nature* **2001**, *410*, 444–446.
14. Fan, H.-M.; Olivo, M.; Shuter, B.; Yi, J.-B.; Bhuvaneswari, R.; Tan, H.-R.; Xing, G.-C.; Ng, C.-T.; Liu, L.; Lucky, S. S.; *et al.* Quantum Dot Capped Magnetite Nanorings as High Performance Nanoprobe for Multiphoton Fluorescence and Magnetic Resonance Imaging. *J. Am. Chem. Soc.* **2010**, *132*, 14803–14811.
15. Perez, M. J.; Josephson, L.; Weissleder, R. Use of Magnetic Nanoparticles as Nanosensors To Probe for Molecular Interactions. *ChemBioChem* **2004**, *5*, 261–264.
16. Park, J.; An, K.; Hwang, Y.; Park, J.-G.; Noh, H.-J.; Kim, J.-Y.; Park, J.-H.; Hwang, N.-M.; Hyeon, T. Ultra-Large-Scale Syntheses of Monodisperse Nanocrystals. *Nat. Mater.* **2004**, *3*, 891–895.
17. Bruchez, M.; Moronne, M.; Gin, P.; Alivisatos, A. P. Semiconductor Nanocrystals as Fluorescent Biological Labels. *Science* **1998**, *281*, 2013–2016.
18. Chan, W. C. W.; Nie, S. Quantum Dot Bioconjugates for Ultrasensitive Nonisotopic Detection. *Science* **1998**, *281*, 2016–2018.
19. Klostranec, J. M.; Chan, W. C. W. Quantum Dots in Biological and Biomedical Research: Recent Progress and Present Challenges. *Adv. Mater.* **2006**, *18*, 1953–1964.
20. Medintz, I. L.; Uyeda, H. T.; Goldman, E. R.; Mattoussi, H. Quantum Dot Bioconjugates for Imaging and Sensing. *Nat. Mater.* **2005**, *4*, 435–446.
21. Hering, V. R.; Gibson, G.; Schumacher, R. I.; Faljoni-Alario, A.; Politi, M. J. Energy Transfer between CdSe/ZnS Core/Shell Quantum Dots and Fluorescent Proteins. *Bioconjugate Chem.* **2007**, *18*, 1705–1708.
22. Mattoussi, H.; Mauro, J. M.; Goldman, E. R.; Anderson, G. P.; Sundar, V. C.; Mikulec, F. V.; Bawendi, M. G. Self-Assembly of CdSe−ZnS Quantum Dot Bioconjugates Using an Engineered Recombinant Protein. *J. Am. Chem. Soc.* **2000**, *122*, 12142–12150.
23. Mamedov, A. A.; Kotov, N. A. Free-Standing Layer-by-Layer Assembled Films of Magnetite Nanoparticles. *Langmuir* **2000**, *16*, 5530–5533.
24. Mamedov, A. A.; Ostrander, J.; Aliev, F.; Kotov, N. A. Stratified Assemblies of Magnetite Nanoparticles and Montmorillonite Prepared by the Layer-by-Layer Assembly. *Langmuir* **2000**, *16*, 3941–3949.
25. Lartigue, L.; Oumzil, K.; Guari, Y.; Larionova, J.; Guérin, C.; Montero, J.-L.; Barragan-Montero, V.; Sangregorio, C.; Caneschi, A.; Innocenti, C.; *et al.* Water-Soluble Rhamnose-Coated Fe_3O_4 Nanoparticles. *Org. Lett.* **2009**, *11*, 2992–2995.
26. Sun, S.; Zeng, H.; Robinson, D. B.; Raoux, S.; Rice, P. M.; Wang, S. X.; Li, G. Monodisperse MFe_2O_4 (M = Fe, Co, Mn) Nanoparticles. *J. Am. Chem. Soc.* **2004**, *126*, 273–279.
27. Hui, C.; Shen, C.; Yang, T.; Bao, L.; Tian, J.; Ding, H.; Gao, H.-J. Large-Scale Fe_3O_4 Nanoparticles Soluble in Water Synthesized by a Facile Method. *J. Phys. Chem. C* **2008**, *112*, 11336–11339.
28. Yi, D. K.; Selvan, T.; Lee, S. S.; Papaefthymiou, G. C.; Kundaliya, D.; Ying, J. Y. Silica-Coated Nanocomposites of Magnetic Nanoparticles and Quantum Dots. *J. Am. Chem. Soc.* **2005**, *127*, 4990–4991.
29. Decher, G. Fuzzy Nanoassemblies: Toward Layered Polymeric Multicomposites. *Science* **1997**, *277*, 1232–1237.
30. Caruso, F.; Caruso, R. A.; Möhwald, H. Nanoengineering of Inorganic and Hybrid Spheres by Colloidal Templating. *Science* **1998**, *282*, 1111–1114.

31. Zhang, X.; Shi, F.; Yu, X.; Liu, H.; Fu, Y.; Wang, Z.; Jiang, L.; Li, X. Polyelectrolyte Multilayer as Matrix for Electrochemical Deposition of Gold Clusters: Toward Super-Hydrophobic Surface. *J. Am. Chem. Soc.* **2004**, *126*, 3064–3065.
32. Lee, J.-S.; Cho, J.; Lee, C.; Kim, I.; Park, J.; Kim, Y.; Shin, H.; Lee, J.; Caruso, F. Layer-by-Layer Assembled Charge-Trap Memory Devices with Adjustable Electronic Properties. *Nat. Nanotechnol.* **2007**, *2*, 790–795.
33. Shiratori, S. S.; Rubner, M. F. pH-Dependent Thickness Behavior of Sequentially Adsorbed Layers of Weak Polyelectrolytes. *Macromolecules* **2000**, *33*, 4213–4219.
34. Dubas, S. T.; Farhat, T. R.; Schlenoff, J. B. Multiple Membranes from "True" Polyelectrolyte Multilayers. *J. Am. Chem. Soc.* **2001**, *123*, 5368–5369.
35. Jiang, C.; Markutsya, S.; Pikus, Y.; Tskruk, V. V. Freely Suspended Nanocomposite Membranes as Highly Sensitive Sensors. *Nat. Mater.* **2004**, *3*, 721–728.
36. Hong, X.; Li, J.; Wang, M.; Xu, J.; Guo, W.; Li, J.; Bai, Y.; Li, T. Fabrication of Magnetic Luminescent Nanocomposites by a Layer-by-Layer Self-Assembly Approach. *Chem. Mater.* **2004**, *16*, 4022–4027.
37. Liu, J.; Zhang, Y.; Yan, C.; Wang, C.; Xu, R.; Gu, N. Synthesis of Magnetic/Luminescent Alginate-Templated Composite Microparticles with Temperature-Dependent Photoluminescence under High-Frequency Magnetic Field. *Langmuir* **2010**, *26*, 19066–19072.
38. Duan, H.; Wang, D.; Kurth, D. G.; Möhwald, H. Directing Self-Assembly of Nanoparticles at Water/Oil Interfaces. *Angew. Chem., Int. Ed.* **2004**, *43*, 5639–5642.
39. Wang, J.; Wang, D.; Sobal, N. S.; Giersig, M.; Jiang, M.; Möhwald, H. Stepwise Directing of Nanocrystals To Self-Assemble at Water/Oil Interfaces. *Angew. Chem., Int. Ed.* **2006**, *45*, 7963–7966.
40. Wang, D.; Duan, H.; Möhwald, H. The Water/Oil Interface: The Emerging Horizon for Self-Assembly of Nanoparticles. *Soft Matter* **2005**, *1*, 412–416.
41. Edwards, E. W.; Wang, D.; Möhwald, H. Hierarchical Organization of Colloidal Particles: From Colloidal Crystallization to Supraparticles Chemistry. *Macromol. Chem. Phys.* **2007**, *208*, 439–445.
42. Tetsuka, H.; Ebina, T.; Mizukami, F. Highly Luminescent Flexible Quantum Dot-Clay Films. *Adv. Mater.* **2008**, *20*, 3039–3043.
43. Cassie, A. B. D.; Baxter, S. Wettability of Porous Surfaces. *Trans. Faraday Soc.* **1944**, *40*, 546–551.
44. Wenzel, R. N. Resistance of Solid Surfaces to Wetting by Water. *Ind. Eng. Chem.* **1936**, *28*, 988–994.
45. Oner, D.; McCarthy, T. J. Ultrahydrophobic Surfaces. Effects of Topography Length Scales on Wettability. *Langmuir* **2000**, *16*, 7777–7782.
46. Blossey, R. Self-Cleaning Surfaces—Virtual Realities. *Nat. Mater.* **2003**, *2*, 301–306.
47. Lau, K. K. S.; Bico, J.; Teo, K. B. K.; Chhowalla, M.; Amaratunge, G. A. J.; Mine, W. I.; Mckinley, G. H.; Gleason, K. K. Superhydrophobic Carbon Nanotube Forests. *Nano Lett.* **2003**, *3*, 1701–1705.
48. Zhai, L.; Cebeci, F. C.; Cohen, R. E.; Rubner, M. F. Stable Superhydrophobic Coatings from Polyelectrolyte Multilayers. *Nano Lett.* **2004**, *4*, 1349–1353.
49. Zhai, L.; Berg, M. C.; Cebeci, F. C.; Kim, Y.; Milwid, J. M.; Rubner, M. F.; Cohen, R. E. Patterned Superhydrophobic Surfaces: Toward a Synthetic Mimic of the Namib Desert Beetle. *Nano Lett.* **2006**, *6*, 1213–1217.
50. Bae, W. K.; Char, K.; Hur, H.; Lee, S. Single-Step Synthesis of Quantum Dots with Chemical Composition Gradients. *Chem. Mater.* **2008**, *20*, 531–539.
51. Buttry, D. *Advances in Electroanalytical Chemistry: Applications of the QCM to Electrochemistry*; Marcel Dekker: New York, 1991.
52. Hemmersam, A. G.; Rechendorff, K.; Besenbacher, F.; Kasemo, B.; Sutherland, D. S. pH-Dependent Adsorption and Conformational Change of Ferritin Studied on Metal Oxide Surfaces by a Combination of QCM-D and AFM. *J. Phys. Chem. C* **2008**, *112*, 4180–4186.
53. Thid, D.; Benkoski, J. J.; Svedhem, S.; Kasemo, B.; Gold, J. DHA-Induced Changes of Supported Lipid Membrane Morphology. *Langmuir* **2007**, *23*, 5878–5881.
54. Höök, F.; Ray, A.; Nordén, B.; Kasemo, B. Characterization of PNA and DNA Immobilization and Subsequent Hybridization with DNA Using Acoustic-Shear-Wave Attenuation Measurements. *Langmuir* **2001**, *17*, 8305–8312.
55. Höök, F.; Kasemo, B.; Nylander, T.; Fant, C.; Sott, K.; Elwing, H. Variations in Coupled Water, Viscoelastic Properties, and Film Thickness of a Mefp-1 Protein Film during Adsorption and Cross-Linking: A Quartz Crystal Microbalance with Dissipation Monitoring, Ellipsometry, and Surface Plasmon Resonance Study. *Anal. Chem.* **2001**, *73*, 5796–5804.